VIII International Conference on Computational Methods in Marine Engineering
MARINE 2019
R. Bensow and J. Ringsberg (Eds)

Effects of Section Geometry on the Energy-saving Rate of PBCF and Model/full-scale Correlation - A CFD Study

Heng Zhang, Xiao-Qian Dong*, Wei Li*, Chen-Jun Yang, Francis Noblesse

(State Key Laboratory of Ocean Engineering,
Collaborative Innovation Center for Advanced Ship and Deep-Sea Exploration
Shanghai Jiao Tong University, Shanghai 200240, China)
E-mail: xiaoqiandong0330@sjtu.edu.cn (X.-Q. D.); wli@sjtu.edu.cn (W.L.)

Key words: PBCF, Section geometry, Scale effect, RANS, CFD

Abstract. The steady flows and hydrodynamic performances of a propeller without and with the Propeller Boss Cap Fins (PBCFs) are simulated by solving the Reynolds-averaged Navier-Stokes (RANS) equations using the software package STAR-CCM$^+$. To determine a suitable grid setting, a grid convergence study is carried out first by changing the grid sizes separately in the sub-domains enclosing the propeller blades and the PBCFs. The CFD investigation into the energy-saving rate of the PBCFs with systematically varied section profiles at model-scale shows the PBCFs with modified 'NACA M7' section geometry performs better than the flat plate in energy-saving effect. Full-scale simulations are also carried out using typical PBCF geometries investigated at model scale, and the results are compared with model-scale ones to evaluate the Reynolds scale effects on the energy-saving rate. The hydrodynamic forces acting on the propeller blades, the PBCFs, and the boss cap are compared to explore the mechanism behind the scale effects on the PBCFs. The study indicates that the scale effect positively influences the energy-saving effect of all the PBCFs investigated, while the flat-plate PBCFs benefit more from the scale effect.

1 INTRODUCTION

As the global warming problem becomes more serious and the energy consumption increases sharply, countries worldwide are paying more attention to the energy problem of shipping industry. In 2011, IMO enacted the Energy Efficiency Design Index (EEDI), which has been enforced since 2013 [1]. Moreover, the recent rise in oil price has also made Energy Saving Devices (ESDs) become a research focus. One of the popular ESDs which has been widely used in vessels is the Propeller Boss Cap Fins (PBCFs) due to its low cost and easy installation. The research of the PBCFs was first introduced by Ouchi *et al.* [2] in 1988. Based on the model tests, they verified that the hub vortex is weakened and the efficiency increases with the installation of the PBCFs. In the tests, the model propeller was located at the downstream of the dynamometer so that the hub vortex can be observed. The test was called the reverse propeller open water test (RPOT) and it has been widely adopted in later studies of the PBCFs.

In the last decade, with the rapid development of computer hardware capability and software technology, Computational Fluid Dynamics (CFD) has become increasingly preferred to evaluate the energy efficiency of ESDs, as it can provide more details of the viscous flow than potential flow methods.

Kai *et al.* [3] divided the propeller and the PBCFs into several parts and analyzed them respectively based on CFD technology. Li *et al.* [4] put forward a design method for the PBCFs based on viscous flow analysis and the lifting line theory. Mizzi *et al.* [5], Seo *et al.* [6] and Lim *et al.* [7] investigated and optimized the influence of design parameter variations for the PBCFs via viscous flow CFD simulations. However, among many of the parameters for PBCFs, the effects of section geometry have hardly been studied in existing studies, and most of the PBCFs take the shape of a flat plate for the convenience and cost-saving of manufacture. As the Computerized Numerical Control technology is widely adopted in propeller manufacture nowadays, machining the PBCFs with a complex geometry becomes relatively easy and inexpensive, which makes it possible to further improve the design of the PBCFs.

It is indicated that the energy saving effect of PBCFs is mostly better at full scale than at model scale [8,9]. Kawamura *et al.* [10] investigated the energy-saving rate of the PBCFs at model and full scale Reynolds numbers with two different inflow conditions by means of CFD analyses. The numerical result showed that the energy-saving rate of the PBCFs at high Reynolds number and non-uniform inflow is larger than that at low Reynolds number and uniform inflow which explains some of the reasons for the higher energy saving effects of PBCFs at full-scale.

This paper presents a CFD study on the energy-saving rate of the PBCFs with systematically varied section profiles, based on the RANS simulations using the software package STAR-CCM$^+$. Firstly, a grid convergence study is carried out by changing the grid sizes separately in the sub-domains enclosing the propeller blades and the PBCFs. Then the RANS simulations are conducted at model scale in steady flows and the hydrodynamic forces are evaluated for different thickness ratios and camber line geometries of the PBCF sections. Furthermore, full-scale simulations are carried out using typical PBCF geometries investigated at model scale. Based on the numerical results, effects of section geometry on the energy-saving rate of PBCFs and model/full-scale correlation are discussed.

2 CFD MODELING APPROACH

2.1 Governing equations

The steady flows and hydrodynamic performances of a propeller without and with the PBCFs were simulated by solving the Reynolds-averaged Navier-Stokes (RANS) equations using the software package STAR-CCM$^+$ version 12.02. The SST k-ω model is employed for turbulence closure, which seems to be mostly used for practical engineering calculations [11]. In all the governing equations, the convection terms are discretized with a second-order upwind scheme and the dissipative terms with a second-order central difference scheme. The overall solution process is based on the SIMPLE algorithm and the gradients are calculated by Green-Gauss techniques.

2.2 Setup of the computational model

The propeller investigated in this paper is DTMB 4381, a five-bladed propeller without skew, presented by Kerwin *et al.* [12]. Table 1 shows the geometric particulars as well as operating conditions of the propeller at model- and full-scale. The square-shaped PBCFs are

adopted in this paper, as illustrated in Figure 1, where the chord length of a fin, c, is 30mm and the height of a fin, d, varies with the radius of the fin. The fins can move relative to the local coordinate system $x'o'y'$ to change its particulars. In order to study the effects of section geometry on the energy-saving rate of PBCFs, the remaining parameters of PBCFs should be consistent. Based on our previous work on the parametric study of the PBCFs, the optimal collection of the PBCFs' design parameters has been found, as listed in Table 2, where the axial distance denotes distance at root between the trailing edge of propeller blade and the leading edge of fin, and the shifting angle denotes the angle between the reference lines of a propeller blade and a fin. In addition, as shown in Figure 2, an S-shaped airfoil profile 'NACA M7' chosen from software Profili Pro is used as the profile of the PBCFs in the grid convergence study presented in Section 2.3.

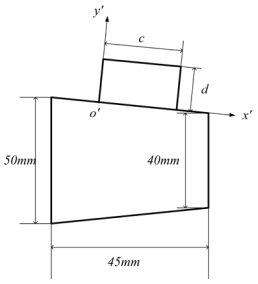

Figure 1: Schematic of the PBCF geometric model.

Figure 2: Geometry of the NACA M7 profile.

Table 1: Particulars of propeller DTMB 4381 at model- and full-scale.

	Model-scale	Full-scale
Scale ratio	20	1
Number of blades	5	
Diameter (m)	0.25	5.0
Boss/diameter ratio	0.2	
Blade area ratio A_E/A_0	0.725	
Rotation	Right-handed	
Velocity of inflow (m/s)	4.445	12.86
Re at 0.75*R*, *J*=0.889	4.2×10^5	2.1×10^7

Table 2: Geometric particulars of the model-scale PBCFs.

Pitch angle	53°
Hub ratio	0.316
Axial distance	15.0 mm
Shifting angle	36°
Skew angle	0°
Profile of fins	Varied
Number of fins	5
Rotation	Right-handed

The computational domain is divided into far, blade and PBCF sub-domains. The inlet and outlet boundaries of the far sub-domain are 5D upstream and 10D downstream of the blade, where D is the propeller diameter. Numerical simulation of the propeller and the PBCFs is based on the multi reference frame (MRF) method, where the far sub-domain is fixed, while

the blade and PBCF sub-domains are rotating. Interfaces are defined between adjacent domains, as shown in Figure 3. The inlet is set as the uniform inflow; the rotating sub-domains are set at a fixed rotation speed, which makes the advance ratio J=0.889 (design condition of DTMB 4381); and the outlet is set as the pressure outlet.

Grids of the three sub-domains are generated separately. The fixed sub-domain is discretized with trimmed grids, and the rotating sub-domains are discretized with polyhedral unstructured grids. Prism layer grids are generated over blade and fin surfaces. The meshing strategy is meant to reduce numerical uncertainties. When changing the geometry of PBCFs, only the grids in the PBCF sub-domain need to be modified while the grids in the remaining sub-domains can be kept unchanged. Grids in the PBCF sub-domain are further refined to make detailed investigation of the flow behind the boss cap. Grids around the tip, trailing edge and leading edge of blades and fins, and the hub surface are all refined since the grid size plays an important role in the CFD simulation of PBCFs. Figure 4 shows the computational meshes in a longitudinal cross section of the computational domain, and on blade and fin surfaces at model-scale. For full-scale simulations, the computational grids, except for those in the prism layers, are scaled up from the model-scale grids. By using the SST k-ω turbulence model, the boundary layer flow is resolved down to the viscous sub-layer at model-scale, while the wall-function approach is employed at full-scale [13]. Therefore, the y^+ on the body surfaces has to be kept within a certain range by using proper prism layer heights. The average values of the y^+ over blade and fin surfaces at mode-scale are approximately equal to 1 and 0.8 respectively, while those at full-scale are approximately equal to 60 and 45 respectively.

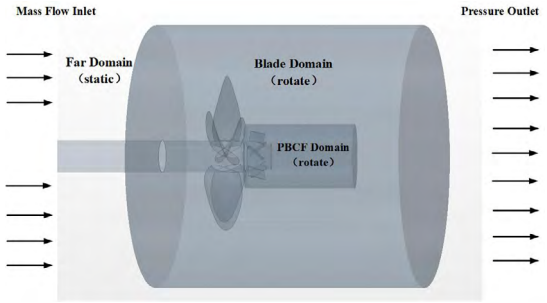

Figure 3: Sub-domains for the propeller and PBCFs.

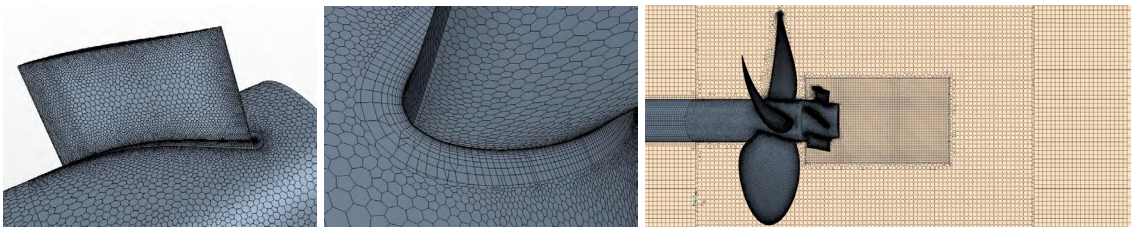

Figure 4: Grids on fin (left) and blade (middle) surfaces, and refined grids in PBCF sub-domain (right).

2.3 Grid convergence study

A grid convergence study is carried out by changing the grid sizes in different sub-domains separately. The convergence properties are investigated for the grids in far and propeller sub-domains firstly. Four sets of grids are generated for the propeller without PBCFs with a

uniform grid refinement ratio of $\sqrt{2}$, except for the prism layer heights which are kept the same to make the y^+ averaged over the body surfaces almost the same for all the grid sets. Table 3 shows the total number of cells in each grid set and the relative changes in K_T and K_Q of the propeller between different grid sets, where i=1 denotes the finest grid set, and i=4 the coarsest grid set. As the grids are refined, the differences in simulated K_T and K_Q become smaller between the successively refined grid sets; in fact, the differences are less than 0.1% between the finest (i=1) and the second finest (i=2) grid sets. To save computer resources, the second finest (i=2) grid set is chosen for far and propeller sub-domains in the following simulations.

Then the grid convergence study is performed for the PBCF sub-domain with four sets of successively refined grids having a uniform grid refinement ratio of $\sqrt{2}$, using the second finest grid set for the far and propeller sub-domains. Table 4 shows the number of cells in the PBCF sub-domain and the relative changes in K_T and K_Q of the fins between different grid sets. Again, it is obvious that the thrust and torque on the PBCFs converge as the grids are refined, and the differences are less than 0.1% between the finest (i=1) and the second finest (i=2) grid sets. Similarly, the second finest grid set (i=2) is chosen for the PBCF sub-domain in the following simulations.

Table 3: Convergence of propeller thrust and torque with the grid size in far and propeller sub-domains.

i	Number of cells (Million)	K_T	$\frac{(K_T)_i}{(K_T)_{i-1}}-1$	$10K_Q$	$\frac{(K_Q)_i}{(K_Q)_{i-1}}-1$	η	$\frac{\eta_i}{\eta_{i-1}}-1$
1	11.93	0.1972		0.4137		0.6745	
2	5.70	0.1973	0.07%	0.4140	0.08%	0.6744	-0.01%
3	3.26	0.1976	0.13%	0.4150	0.24%	0.6737	-0.10%
4	1.86	0.1979	0.16%	0.4161	0.27%	0.6730	-0.11%

Table 4: Convergence of fin thrust and torque with the grid size in PBCF sub-domain.

i	Number of cells (Million)	K_T	$\frac{(K_T)_i}{(K_T)_{i-1}}-1$	$10K_Q$	$\frac{(K_Q)_i}{(K_Q)_{i-1}}-1$
1	2.53	-0.005078		-0.007638	
2	1.34	-0.005074	-0.08%	-0.007633	-0.06%
3	0.73	-0.005090	0.32%	-0.007648	0.20%
4	0.46	-0.005123	0.64%	-0.007691	0.57%

3 EFFECTS OF SECTION GEOMETRY AT MODEL-SCALE

3.1 Selection of section geometry and analytical method

To investigate the effect of section geometry on the energy-saving rate of the PBCFs, systematically varied section profiles are adopted for the PBCFs. In this paper, we choose the S-shaped airfoil profile 'NACA M7' (abbreviated as 'M7' hereinafter) as the baseline of the fins, of which the maximum camber ratio, f_{max}/c, is -0.05 and the maximum camber ratio, t_{max}/c, is 0.0619. It is noted that the fins are cambered towards the face side, as they experience a negative angle of attack. Three camber lines, named respectively as 'mod1',

'mod2', and 'mod3', are generated using based on the baseline 'M7'. When the camber line is normalized with the maximum camber, they have the same camber distribution. The f_{max}/c of 'mod1', 'mod2' and 'mod3' is 0.025, 0.035, and 0.08 respectively. The camber line 'mod4' has the same f_{max}/c as the baseline (which is 0.05), while its S-shaped tail is more curved. The camber line 'flat' denotes the flat plate. Figure 5 illustrates the above-mentioned camber lines, where the y coordinate has been magnified tenfold. Two types of thickness distributions are adopted including that of the baseline and the flat plate, named as 'M7' and 'flat' respectively. The maximum thickness of the fins is 1.5mm. According to different combinations of camber lines and thickness distributions, twelve types of the PBCFs are generated, named by A-B, where 'A' denotes the camber line type and 'B' denotes the thickness distribution. The edges and corners of the PBCFs with thickness distributions of 'flat' are rounded.

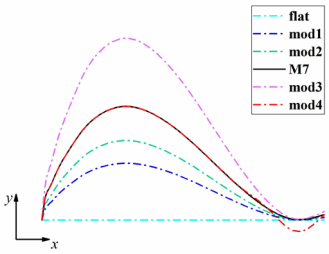

Figure 5: Schematic of systematically varied camber lines.

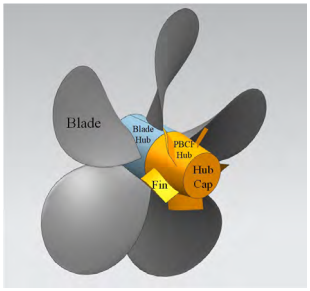

Figure 6: Definition of each part of the propeller and PBCFs.

To investigate the interactions between the propeller, the boss, and the PBCFs in detail, the hydrodynamic forces on the various parts as marked out in Figure 6 are analyzed. The thrust and torque coefficients are decomposed as

$$\left.\begin{aligned} K_T &= K_T^B + K_T^F + K_T^{BH} + K_T^{FH} + K_T^C \\ K_Q &= K_Q^B + K_Q^F \end{aligned}\right\} \tag{1}$$

where superscript *B, F, BH, FH* and *C* denote the blade, fin, blade hub, fin hub and hub cap, respectively. The relative changes in thrust and torque coefficients are defined as

$$\left.\begin{aligned} \Delta K_T &= \frac{K_T' - K_T}{K_T} \\ \Delta K_Q &= \frac{K_Q' - K_Q}{K_Q} \end{aligned}\right\} \tag{2}$$

where K_T' and K_Q' denote the thrust and torque coefficients of the propeller with PBCFs, and

K_T and K_Q denote the thrust and torque coefficients of the propeller without PBCFs.

The energy-saving rate is defined as

$$\Delta\eta=\frac{\eta'-\eta}{\eta} \tag{3}$$

where η' denotes the efficiency of the propeller with PBCFs and η denotes the efficiency of the propeller without PBCFs.

3.2 Analysis of PBCF's energy-saving mechanism

Table 5 and Table 6 show the model-scale CFD simulation results of the gains in K_T, K_Q and η for the DTMB 4381 propeller fitted with the PBCFs having different section geometries. The differences in $\Delta\eta$ between Table 5 and Table 6 indicate that thickness distribution of 'M7' performs better in energy-saving effect than the 'flat' thickness distribution. As seen in Figure 7, flow separation occurs near the leading edge of the PBCF with 'flat-flat' camber and thickness distributions, but it does not occur in the case of 'mod1-M7'. Consequently, the fin drags ΔK_T^F with the 'flat' thickness distribution in Table 6 are all larger than those with the 'M7' thickness in Table 5. Comparing the $\Delta\eta$ with different fin section geometries, it is found that appropriate camber lines for both 'M7' and 'flat' thickness distributions can further improve the energy-saving rate. The camber ratios 0.025 and 0.035 are the most suitable for the S-shaped camber line while larger camber ratio 0.08 has relatively poor performance on the energy-saving rate. The larger camber ratio generates higher lift and drag, so that both thrust and torque of the PBCFs increase. Because the thrust in 'mod4-M7' case occupies larger proportion than torque, the energy saving performance of the PBCF in that case is not so good. And compared with 'M7-M7' and 'mod4-M7' PBCFs, the modification of S-shaped tail has no obvious influence on the energy-saving rate.

In order to analyze the flow fields with diferent PBCFs, circumferentially averaged velocity profiles at different axial stations are shown in Figure 8, where V_a and V_t denote respectively the axial and tangential flow velocities, and V denotes the advance speed. As seen in Figure 8(a), the axial flow slows down a little due to the blockage effect of PBCFs, which results in the increases in K_T^B and K_Q^B. A significant decrease in the tangential induced velocity and a slight decrease in the axial velocity within range of the fin and hub cap can be seen in Figure 8(b). The decrease in tangential velocity in the wake means the hub vortex behind the hub cap is greatly eliminated, as seen in Figure 9. Because of the elimination of hub vortex, the pressure resistance on the hub cap is reduced, as K_T^C greatly increases. However, the energy-saving rate of 'mod3-M7' case is the lowest, although the induced velocities in that case are lower than in other cases, which seems to suggest that the energy-saving effect cannot be evaluated only by the reduction in the tangential induced velocities in the slipstream.

Table 5: CFD results of PBCFs with thickness distributions of 'M7' for the propeller at model-scale.

Relative value (%)	flat-M7	mod1-M7	mod2-M7	M7-M7	mod3-M7	mod4-M7
ΔK_T^B	0.61	0.61	0.61	0.63	0.72	0.62
ΔK_T^F	-2.43	-2.46	-2.53	-2.65	-3.10	-2.58
ΔK_T^{BH}	0.01	0.01	0.01	0.01	0.01	0.01
ΔK_T^{FH}	0.19	0.22	0.23	0.24	0.25	0.24
ΔK_T^C	2.75	2.78	2.80	2.80	2.84	2.81
ΔK_T	1.13	1.16	1.13	1.03	0.71	1.09
ΔK_Q^B	0.27	0.26	0.25	0.25	0.30	0.25
ΔK_Q^F	-1.72	-1.80	-1.82	-1.84	-1.94	-1.78
ΔK_Q	-1.45	-1.54	-1.57	-1.59	-1.64	-1.53
$\Delta\eta$	2.62	2.75	2.74	2.66	2.39	2.66

Table 6: CFD results of PBCFs with thickness distributions of 'flat' for the propeller at model-scale.

Relative value (%)	flat-flat	mod1-flat	mod2-flat	M7-flat	mod3-flat	mod4-flat
ΔK_T^B	0.64	0.65	0.66	0.70	0.75	0.71
ΔK_T^F	-2.63	-2.74	-2.79	-2.90	-3.25	-3.00
ΔK_T^{BH}	0.01	0.01	0.01	0.01	0.01	0.01
ΔK_T^{FH}	0.19	0.21	0.22	0.23	0.25	0.24
ΔK_T^C	2.77	2.79	2.79	2.84	2.85	2.83
ΔK_T	0.97	0.91	0.88	0.88	0.61	0.78
ΔK_Q^B	0.27	0.27	0.27	0.30	0.31	0.29
ΔK_Q^F	-1.63	-1.76	-1.78	-1.84	-1.90	-1.86
ΔK_Q	-1.35	-1.49	-1.51	-1.54	-1.59	-1.57
$\Delta\eta$	2.36	2.44	2.43	2.46	2.24	2.38

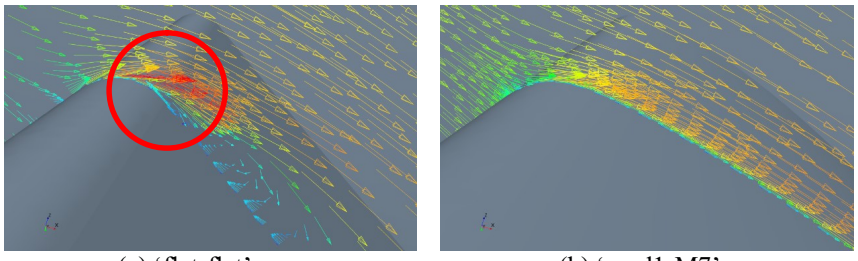

(a) 'flat-flat' (b) 'mod1-M7'

Figure 7: Relative flow velocities around the mid-span section of the PBCFs at model scale.

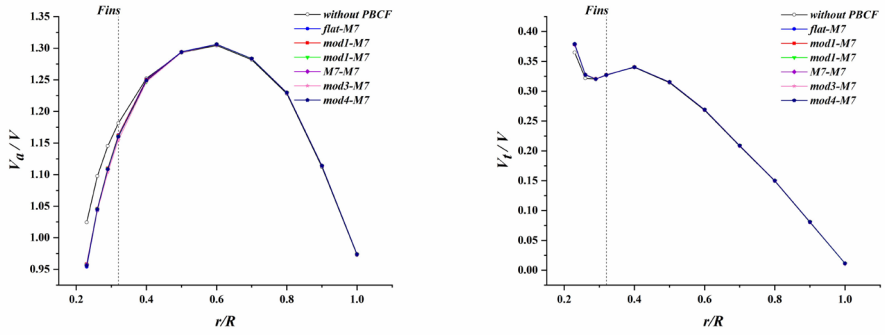

(a) At the station in the middle of propeller and PBCF,

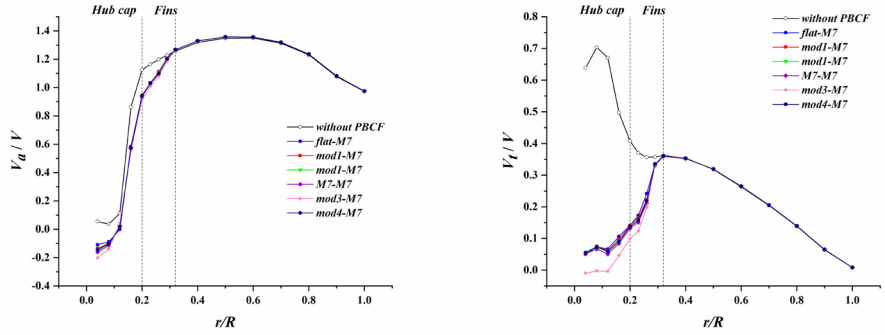

(b) 0.02D downstream from the end of the hub cap,

Figure 8: Radial distributions of circumferentially averaged velocities, axial component (left) and tangential component (right).

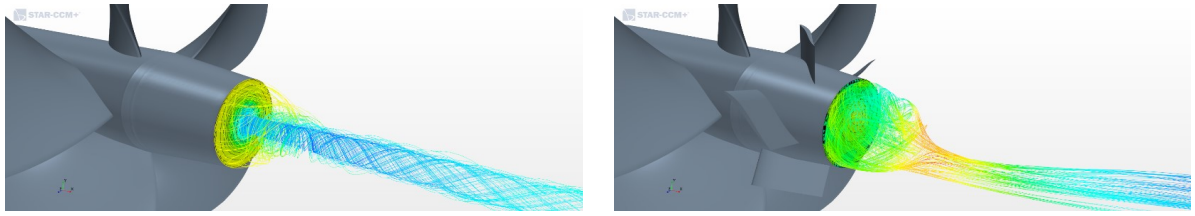

Figure 9: Streamlines behind the hub cap without PBCF and with 'mod1-M7' PBCF.

4 SCALE EFFECT

Tables 7 and 8 show the CFD simulation results of the components of PBCFs with different section geometries at full scale. Comparing the model- and full-scale open water performances of the propeller and PBCFs in Tables 5 through 8, the full-scale $\Delta\eta$ for all the PBCFs at the design point are 0.13%~0.35% higher than corresponding model-scale results. The conclusion about geometry effect drawn at model-scale also applies to full-scale, the appropriate camber ratio can improve the performance of PBCF and camber line 'mod1' is the most effective. In addition, different section profile has different scale effect, where the energy-saving rate with the thickness distribution of 'flat' has a higher increase than 'M7' at full-scale. As it can be seen, the energy-saving rate of PBCFs with 'flat-flat' and 'flat-M7' are almost equal at full-scale. The negative thrust of PBCFs with thickness distribution of 'flat'

increase not as much as 'M7', because the flow separation in 'flat' cases at model-scale disappear at full-scale due to fully developed turbulent flow, as seen in Figure 10. The distinctions of the scale effects are mainly in hydrodynamic performance of the fins. Both thrust and torque of the fins increase at full-scale, while torque contributes more to the efficiency improvement. To better understand scale effects in Reynolds number, the open water performances of the propeller and typical PBCFs are divided into pressure and viscous components in Table 9. The scale effect on both thrust and torque of fins can mainly attribute to pressure components partly as a result of reduced boundary layer thickness on full-scale fin surfaces [13].

Table 7: CFD results of PBCFs with thickness distributions of 'M7' for the propeller at full-scale.

Relative value (%)	flat-M7	mod1-M7	mod2-M7	M7-M7	mod3-M7	mod4-M7
ΔK_T^B	0.70	0.68	0.68	0.73	0.79	0.69
ΔK_T^F	-2.66	-2.69	-2.76	-2.86	-2.29	-2.68
ΔK_T^{BH}	0.00	0.00	0.00	0.00	0.00	0.00
ΔK_T^{FH}	0.22	0.25	0.25	0.26	0.28	0.26
ΔK_T^C	2.67	2.71	2.70	2.71	2.76	2.71
ΔK_T	0.93	0.95	0.87	0.84	0.64	0.98
ΔK_Q^B	0.34	0.31	0.31	0.35	0.37	0.32
ΔK_Q^F	-2.11	-2.22	-2.26	-2.27	-2.26	-2.13
ΔK_Q	-1.77	-1.91	-1.95	-1.92	-1.89	-1.81
$\Delta\eta$	2.75	2.92	2.88	2.82	2.57	2.84

Table 8: CFD results of PBCFs with thickness distributions of 'flat' for the propeller at full-scale.

Relative value (%)	flat-flat	mod1-flat	mod2-flat	M7-flat	mod3-flat	mod4-flat
ΔK_T^B	0.64	0.70	0.71	0.76	0.78	0.72
ΔK_T^F	-2.49	-2.70	-2.79	-2.86	-3.13	-2.83
ΔK_T^{BH}	0.00	0.00	0.00	0.00	0.00	0.00
ΔK_T^{FH}	0.23	0.24	0.25	0.27	0.28	0.26
ΔK_T^C	2.66	2.69	2.69	2.77	2.79	2.71
ΔK_T	1.04	0.93	0.87	0.93	0.73	0.85
ΔK_Q^B	0.30	0.33	0.33	0.36	0.36	0.33
ΔK_Q^F	-1.92	-2.04	-2.10	-2.13	-2.17	-2.05
ΔK_Q	-1.62	-1.71	-1.76	-1.77	-1.81	-1.71
$\Delta\eta$	2.71	2.69	2.68	2.75	2.58	2.61

Table 9: Pressure and viscous components of the effect of PBCFs for the propeller.

Relative value (%)	Model-scale				Full-scale			
	flat-flat		mod1-M7		flat-flat		mod1-M7	
	pressure	viscous	pressure	viscous	pressure	viscous	pressure	viscous
ΔK_T^B	0.63	0.01	0.60	0.01	0.64	0.00	0.67	0.00
ΔK_T^F	-2.54	-0.10	-2.35	-0.11	-2.44	-0.05	-2.64	-0.05
ΔK_T^{BH}	0.00	0.01	0.00	0.01	0.00	0.00	0.00	0.00
ΔK_T^{FH}	0.17	0.02	0.20	0.02	0.22	0.01	0.24	0.01
ΔK_T^C	2.77	0.00	2.78	0.00	2.66	0.00	2.71	0.00
ΔK_Q^B	0.28	-0.01	0.27	-0.01	0.30	0.00	0.31	0.00
ΔK_Q^F	-1.68	0.03	-1.87	0.04	-1.94	0.02	-2.24	0.02

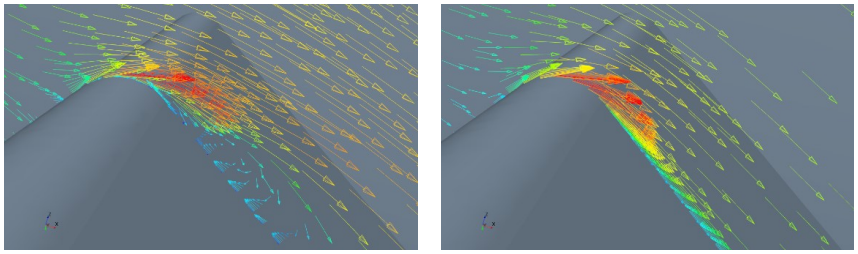

(a) at model-scale (b) at full-scale

Figure 10: Relative velocity vectors on the 0.5d section of the 'flat-flat' PBCF

5 CONCLUSIONS

Based on the RANS simulations, the effects of section geometry and model/full scale correlation of the PBCF have been numerically studied. A grid convergence study was carried out first by changing the grid sizes separately enclosing the propeller and PBCFs to determine appropriate grid sizes. By analyzing the hydrodynamic performances of each part of the propeller and PBCFs with different section profiles at model-scale, the PBCFs with modified 'NACA M7' section geometry showed a better energy-saving performance than the flat plate section. It is found that the S-shaped camber line with an appropriate camber ratio could further improve the energy-saving rate. The flow field characteristic of PBCFs also inferred that the energy saving effect cannot be evaluated only by the velocity reduction in the wake field.

The hydrodynamic performances at model- and full-scale were investigated using typical PBCF geometries. High Reynolds number had the positive influence on the energy-saving effect for all the PBCFs. The section geometry effect at model-scale also agreed with that at full-scale. From the viscous CFD results, PBCFs with different section geometries had different scale effects, which suggests that the design of ESDs should be carried out at full-scale condition when it is possible. Future studies will take the presence of the wake of the hull into consideration at full-scale and more effective section geometry for the PBCFs will be exploited.

REFERENCES

[1] MEPC. The Marine Environment Protection Committee Resolution. (2011).

[2] Ouchi, K.; Ogura, M.; Kono, Y.; Orito, H.; Shiotsu, T.; Tamashima, M. and Koizuka, H. A research and development of PBCF (propeller boss cap fins). *Journal of the Society of Naval Architects of Japan* (1988) **163**:66-78.

[3] Kai, H.; Bito, S. and Miura, Y. Study on clarification of hydrodynamic mechanisms of PBCF by CFD. *Journal of the Japan Society of Naval Architects and Ocean Engineers* (2009) **12(10)**:37-47.

[4] Li, P.C.; Zhou, W.X. and Dong S.T. A design method of propeller boss cap fins (PBCF). *China Shipbuilding* (2014) **55(01)**:19-27.

[5] Mizzi, K.; Demirel, Y.K.; Banks, C.; Turan, O.; Kaklis, P. and Atlar, M. Design optimisation of propeller boss cap fins for enhanced propeller performance. *Applied Ocean Research* (2017) **62**:210-222.

[6] Seo, J.; Lee, S.J.; Han, B. and Rhee, S.H. Influence of design parameter variations for Propeller-Boss-Cap-Fins on hub vortex reduction. *Journal of Ship Research* (2016) **60(4)**:203-218.

[7] Lim, S.S.; Kim, T.W.; Lee, D.M.; Kang, C.G. and Kim, S.Y. Parametric study of propeller boss cap fins for container ships. *International Journal of Naval Architecture and Ocean Engineering* (2014) **6(2)**:187-205.

[8] Nojiri, T.; Ishii, N. and Kai, H. Energy saving technology of propeller boss cap fins (PBCF) and its evolution. *J JIME* (2011) **46(3)**:350-358.

[9] Hansen, H.R.; Dinham-Peren, T. and Nojiri, T. Model and full scale evaluation of a 'propeller boss cap fins' device fitted to an Aframax tanker. In Second International Symposium on Marine Propulsors, smp'11, Hamburg, Germany (2011)

[10] Kawamura, T.; Ouchi, K. and Nojiri, T. Model and full scale CFD analysis of propeller boss cap fins (PBCF). *Journal of marine science and technology* (2012) **17(4)**: 469-480.

[11] Morgut, M. and Nobile, E. Influence of grid type and turbulence model on the numerical prediction of the flow around marine propellers working in uniform inflow. *Ocean Engineering* (2012) **42**:26-34.

[12] Kerwin, J.E. and Lee, C.S. Prediction of steady and unsteady marine propeller performance by numerical lifting-surface theory. *Sname Transactions* (1978) **86**:1-30.

[13] Dong, X.Q.; Li, W.; Yang, C.J. and Noblesse, F. RANSE-based Simulation and Analysis of Scale Effects on Open-Water Performance of the PPTC-II Benchmark Propeller. *Journal of Ocean Engineering and Science* (2018) **3(3)**:186-204.